A direct test of density wave theory in grand-design spiral galaxies

Thomas Peterken[1], Michael Merrifield[1], Alfonso Aragón-Salamanca[1], Niv Drory[2], Coleman Krawczyk[3], Karen Masters[3, 4], Anne-Marie Weijmans[5], and Kyle Westfall[6]

[1]*School of Physics and Astronomy, The University of Nottingham, University Park, Nottingham NG7 2RD, UK*

[2]*McDonald Observatory, The University of Texas at Austin, 1 University Station, Austin, TX 78712, USA*

[3]*Institute of Cosmology & Gravitation, University of Portsmouth, Dennis Sciama Building, Portsmouth, PO1 3FX, UK*

[4]*Haverford College, Department of Physics and Astronomy, 370 Lancaster Avenue, Haverford, Pennsylvania 19041, USA*

[5]*School of Physics and Astronomy, University of St Andrews, North Haugh, St Andrews, KY16 9SS, UK*

[6]*University of California Observatories, University of California, Santa Cruz, Santa Cruz, CA 95064, USA*

While the defining features of spiral galaxies are the beautiful arms that they display, the exact nature of such spiral structures is still an open question[1]. Since the 1960s, it has been widely assumed that spiral arms in galaxies with two distinct symmetrical arms (known as "grand design" systems[2]) are the products

of density waves that propagate around the disk as a persistent pattern, with the spiral arms being visibly enhanced by the star formation that is triggered as the passing wave compresses gas in the galaxy disk[1,3]. Such a persistent wave would propagate with an approximately constant angular speed called its pattern speed, Ω_P, and so a simple test of the density-wave theory is to measure this quantity and show that it does not vary with radius in the galaxy. Unfortunately, this measurement is difficult because Ω_P only has an indirect connection to readily-measurable quantities such as the stellar rotation speed.[4–8] Here, we make use of the detailed information on stellar populations that can now be extracted from spectral mapping of a grand-design spiral galaxy (UGC 3825) to measure the offset between young stars of a known age and the spiral arm in which they formed, allowing the first direct measure of Ω_P at a range of radii. The offset in this galaxy is found to be as expected for a pattern speed that varies little with radius, vindicating the global spiral density wave theory and establishing the reliability of this new method.

The idea of using offsets between features of differing ages to determine pattern speeds is not new; it has been employed to good effect using the observed offset between the dense molecular gas that is currently being compressed by the spiral wave and young hot stars that formed previously in the spiral arm and have now moved from the peak of the wave.[9–12] However, in these previous analyses the offset in time between the two phases – essentially the timescale for star formation – was also unknown, so had to be solved for simultaneously. The

price paid for deriving this extra parameter was that Ω_P had to be assumed to be constant with radius, making it less of a test of the persistent density wave picture. However, we have now reached a point where the quality of optical spectroscopy and the associated modelling techniques allow one to extract a stellar population of a specified age from spectral data, so that Ω_P can be measured as a function of radius to see how constant it really is.

As a test case, we have selected the galaxy UGC 3825. This isolated system[13] has a symmetric grand-design structure, which makes it a prime candidate for being the product of a global density wave. According to the Galaxy Zoo citizen science project [14], it does not contain a bar, which might complicate the interpretation of its spiral structure, and it is at an ideal intermediate angle to the line of sight, allowing us both to identify its spiral structure and to measure the rotational motion of material via the Doppler shift. It is also one of the targets of the SDSS-IV MaNGA (Mapping Nearby Galaxies at APO) integral-field spectroscopic survey,[15] which means that for every point across the face of the galaxy a high-quality spectrum has been obtained.[16]

At each location across the face of the galaxy, we decompose the MaNGA spectrum into the contributions from stars of differing ages[17,18] and that from current star formation[19,20] (see Methods), allowing us to map the distribution of all these various components. Figure 1 shows the resulting distribution of young stars and star formation. The young stars were chosen to be those with ages between 20 and 60 million years, but since the youngest stars dominate the light, the map picks out the location of the stars at a time $\delta\tau \sim 2 \times 10^7$

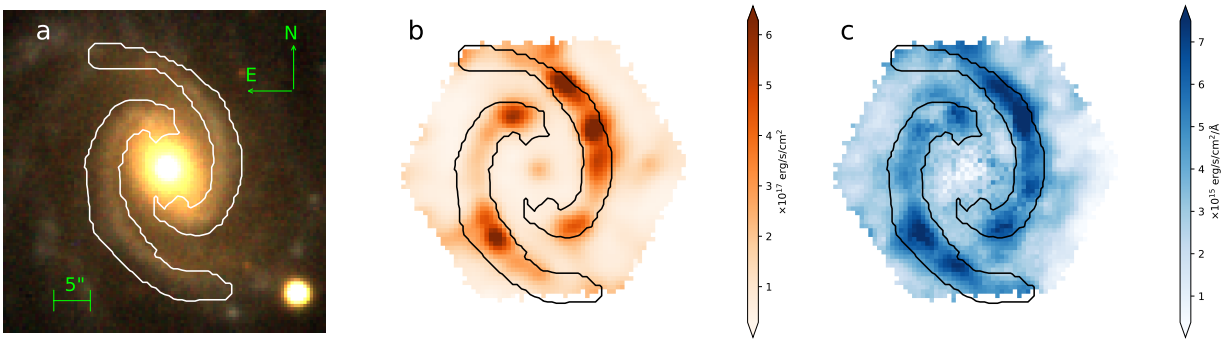

Figure 1: UGC 3825. *Left*: SDSS imagery[21]. *Centre*: Ongoing star-formation, traced by the Hydrogen-α emission line. *Right*: contribution of young stars. The outline denotes the region within which at least 25% of GZ:3D users agreed on the presence of a spiral arm.

years after they formed.[1] As a fiducial, the figure also shows the location of the spiral arm regions determined as part of the ongoing Galaxy Zoo:3D (GZ:3D) citizen science project[2] (see Methods for details). Even in these raw maps, it is discernable that over most of the galaxy the young stellar population is found on the leading edge of the spiral arm. This is what one would expect from the spiral density wave picture, as the material in the inner parts of a galaxy is predicted to circulate at a higher angular velocity than the spiral pattern, so gas clouds overtake the arms and collapse to form stars in the density wave. These young stars continue to overtake the spiral arm to emerge out of the leading edge after a time interval determined by the difference between the pattern and material speeds.

We can render this description more quantitative by measuring the small angular offset

[1]There is some uncertainty in the value adopted here, but it is notable that if it is left as a free parameter in the analysis then this is also the value that returns the most consistent estimate for Ω_p at all radii.

[2]`https://www.zooniverse.org/projects/klmasters/galaxy-zoo-3d`

in azimuth between these two spiral arm tracers as a function of radius, $\delta\theta(r)$, by cross correlating data from the maps of current star formation and the young stellar population. We can also measure the circular angular speed of the galaxy as a function of radius, $\Omega(r)$, using the Doppler shift in the emission lines in the spectra (appropriately corrected for the galaxy's inclination; see Methods for details). By considering the rate at which material travelling around the galaxy at this angular speed will overtake the spiral pattern, it is straightforward to show[10] that the pattern speed is given by the formula

$$\Omega_{\rm P}(r) = \Omega(r) - \frac{\delta\theta}{\delta\tau}(r). \qquad (1)$$

The results of this analysis for UGC 3825, presented in Figure 2, are entirely consistent with the predictions of the density wave theory. At small radii, as expected from the qualitative analysis of offsets, matter is rotating faster than the derived pattern speed, but eventually the measured angular speed of material drops to where it is rotating at the same speed as the spiral pattern, a point known as the corotation resonance. The location of this resonance, at a radius of $\sim 6\,$kpc, is consistent with estimates for other galaxies using less direct techniques[11], and approximately corresponds to where the arm-interarm flux contrast is greatest, as predicted by simulations[22]. The derived form for $\Omega_{\rm P}(r)$ is consistent with a constant value of $31\,{\rm km\,s^{-1}kpc^{-1}}$. Such constancy was in no way imposed by the analysis, but rather again confirms the predictions of density wave theory for this galaxy.

Thus, at least for the case of UGC 3825, a coherent story emerges in which the observed spiral structure is consistent with the predictions of simple density wave theory. However, it has been suggested[23] (and evidence is making it increasingly clear[24,25]) that such a model

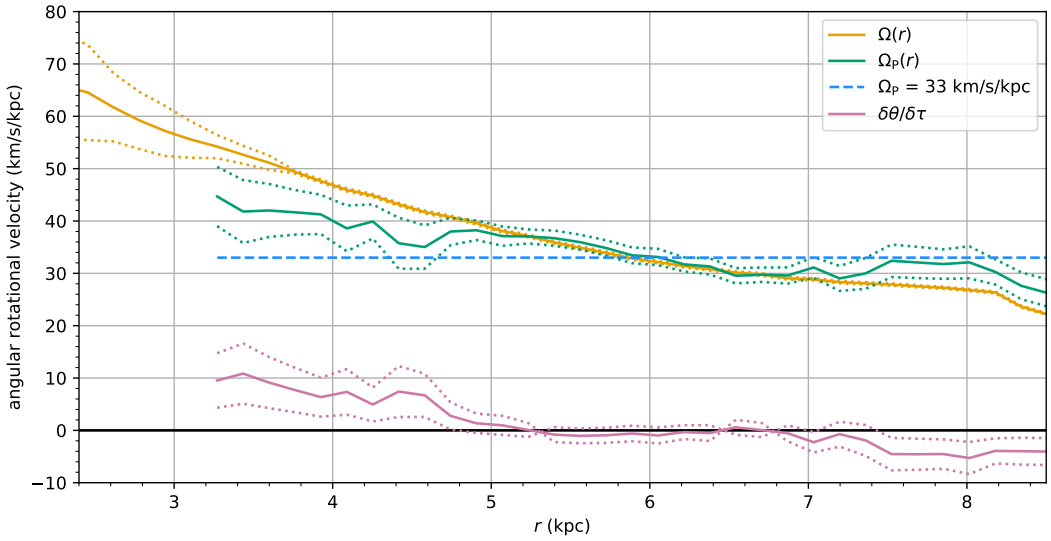

Figure 2: Pattern speed $\Omega_{\rm P}(r)$ (blue solid), which is the value of $\frac{\delta\theta}{\delta\tau}(r)$ (red solid) subtracted from the angular velocity of material $\Omega(r)$ (orange solid), as defined in Equation 1. The estimated uncertainties in these quantities are denoted by dotted lines (see Methods for details). The light blue dashed line shows a best-fit flat line to the pattern speed. The pattern-speed calculation is limited to the region where at least 25% of the GZ:3D users agree on the location of the spiral arms.

can only explain the spiral structure found in a fraction of all galaxies. Since different mechanisms for producing spiral arms should result in significantly different radial profiles in pattern speed,[26] we can distinguish between such physical processes using this new technique; large spectroscopic surveys of galaxies like MaNGA will ultimately allow us to fully determine the circumstances under which galaxy spiral arms are produced by long-lived density waves.

1. Dobbs, C. & Baba, J. Dawes Review 4: Spiral Structures in Disc Galaxies. *Publ. Astron. Soc. Aust.* **31**, e035 (2014). 1407.5062.

2. Elmegreen, D. M. & Elmegreen, B. G. Flocculent and grand design spiral structure in field, binary and group galaxies. *Mon. Not. R. Astron. Soc.* **201**, 1021–1034 (1982).

3. Lin, C. C. & Shu, F. H. On the Spiral Structure of Disk Galaxies, II. Outline of a Theory of Density Waves. *Proc. Nat. Acad. Sci. USA* **55**, 229–234 (1966).

4. Tremaine, S. & Weinberg, M. D. A kinematic method for measuring the pattern speed of barred galaxies. *Astrophys. J. Lett.* **282**, L5–L7 (1984).

5. Merrifield, M. R. & Kuijken, K. The pattern speed of the bar in NGC 936. *Mon. Not. R. Astron. Soc.* **274**, 933–938 (1995). astro-ph/9502069.

6. Debattista, V. P. On position angle errors in the Tremaine-Weinberg method. *Mon. Not. R. Astron. Soc.* **342**, 1194–1204 (2003). astro-ph/0401137.

7. Font, J. *et al.* Resonant Structure in the Disks of Spiral Galaxies, Using Phase Reversals in Streaming Motions from Two-dimensional Hα Fabry-Perot Spectroscopy. *Astrophys. J. Lett.* **741**, L14 (2011). 1109.5574.

8. Beckman, J. E., Font, J., Borlaff, A. & García-Lorenzo, B. Precision Determination of Corotation Radii in Galaxy Disks: Tremaine-Weinberg versus Font-Beckman for NGC 3433. *Astrophys. J.* **854**, 182 (2018). 1801.07476.

9. Egusa, F., Sofue, Y. & Nakanishi, H. Offsets between Hα and CO Arms of a Spiral Galaxy, NGC 4254: A New Method for Determining the Pattern Speed of Spiral Galaxies. *Publ. Astron. Soc. Jpn.* **56**, L45–L48 (2004). astro-ph/0410469.

10. Egusa, F., Kohno, K., Sofue, Y., Nakanishi, H. & Komugi, S. Determining Star Formation Timescale and Pattern Speed in Nearby Spiral Galaxies. *Astrophys. J.* **697**, 1870–1891 (2009). 0904.3121.

11. Tamburro, D. *et al.* Geometrically Derived Timescales for Star Formation in Spiral Galaxies. *Astron. J.* **136**, 2872–2885 (2008). 0810.2391.

12. Egusa, F., Koda, J. & Scoville, N. Molecular Gas Evolution Across a Spiral Arm in M51. *Astrophys. J.* **726**, 85 (2011). 1011.3889.

13. Verley, S. *et al.* The AMIGA sample of isolated galaxies. V. Quantification of the isolation. *Astron. & Astrophys.* **472**, 121–130 (2007). 0706.2555.

14. Hart, R. E. *et al.* Galaxy Zoo: comparing the demographics of spiral arm number and a new method for correcting redshift bias. *Mon. Not. R. Astron. Soc.* **461**, 3663–3682 (2016). 1607.01019.

15. Bundy, K. *et al.* Overview of the SDSS-IV MaNGA Survey: Mapping nearby Galaxies at Apache Point Observatory. *Astrophys. J.* **798**, 7 (2015). 1412.1482.

16. Drory, N. *et al.* The MaNGA Integral Field Unit Fiber Feed System for the Sloan 2.5 m Telescope. *Astron. J.* **149**, 77 (2015). 1412.1535.

17. Conroy, C. Modeling the Panchromatic Spectral Energy Distributions of Galaxies. *Ann. Rev. Astron. Astrophys.* **51**, 393–455 (2013). 1301.7095.

18. Cid Fernandes, R., Mateus, A., Sodré, L., Stasińska, G. & Gomes, J. M. Semi-empirical analysis of Sloan Digital Sky Survey galaxies - I. Spectral synthesis method. *Mon. Not. R. Astron. Soc.* **358**, 363–378 (2005). astro-ph/0412481.

19. Kennicutt, R. C., Jr. Star Formation in Galaxies Along the Hubble Sequence. *Ann. Rev. Astron. Astrophys.* **36**, 189–232 (1998). astro-ph/9807187.

20. Cappellari, M. & Emsellem, E. Parametric Recovery of Line-of-Sight Velocity Distributions from Absorption-Line Spectra of Galaxies via Penalized Likelihood. *Publ. Astron. Soc. Pac.* **116**, 138–147 (2004). astro-ph/0312201.

21. Fukugita, M. *et al.* The Sloan Digital Sky Survey Photometric System. *Astron. J.* **111**, 1748 (1996).

22. Sellwood, J. A. & Carlberg, R. G. Transient Spirals as Superposed Instabilities. *Astrophys. J.* **785**, 137 (2014). 1403.1135.

23. Fridman, A. M., Polyachenko, V. L. & Zasov, A. V. On Some Observational Restrictions to Galactic Spiral Structure Theories. In Combes, F. & Casoli, F. (eds.) *Dynamics of Galaxies and Their Molecular Cloud Distributions*, vol. 146 of *IAU Symp.*, 109 (1991).

24. Meidt, S. E., Rand, R. J. & Merrifield, M. R. Uncovering the Origins of Spiral Structure by Measuring Radial Variation in Pattern Speeds. *Astrophys. J.* **702**, 277–290 (2009). 0907.3443.

25. Hart, R. E. *et al.* Galaxy Zoo and SPARCFIRE: constraints on spiral arm formation mechanisms from spiral arm number and pitch angles. *Mon. Not. R. Astron. Soc.* **472**, 2263–2279 (2017). 1708.04628.

26. Baba, J., Morokuma-Matsui, K. & Egusa, F. Radial distributions of arm-gas offsets as an observational test of spiral theories. *Publ. Astron. Soc. Jpn.* **67**, L4 (2015). 1505.02881.

27. Taylor, M. B. TOPCAT and STIL: Starlink Table/VOTable Processing Software. In Shopbell, P., Britton, M. & Ebert, R. (eds.) *Astronomical Data Analysis Software and Systems XIV*, vol. 347 of *Astro. Soc. P.*, 29 (2005).

28. The Astropy Collaboration *et al.* The Astropy Project: Building an inclusive, open-science project and status of the v2.0 core package. *ArXiv e-prints* (2018). 1801.02634.

29. Jones, E., Oliphant, T., Peterson, P. *et al.* SciPy: Open source scientific tools for Python (2001–). URL http://www.scipy.org/. [Online; accessed <today>].

30. Hunter, J. D. Matplotlib: A 2D Graphics Environment. *Comput. Sci. Eng.* **9**, 90–95 (2007).

31. Blanton, M. R. *et al.* Sloan Digital Sky Survey IV: Mapping the Milky Way, Nearby Galaxies, and the Distant Universe. *Astron. J.* **154**, 28 (2017). 1703.00052.

32. Yan, R. *et al.* SDSS-IV MaNGA IFS Galaxy Survey: Survey Design, Execution, and Initial Data Quality. *Astron. J.* **152**, 197 (2016). 1607.08613.

33. Law, D. R. *et al.* The Data Reduction Pipeline for the SDSS-IV MaNGA IFU Galaxy Survey. *Astron. J.* **152**, 83 (2016). 1607.08619.

34. Law, D. R. *et al.* Observing Strategy for the SDSS-IV/MaNGA IFU Galaxy Survey. *Astron. J.* **150**, 19 (2015). 1505.04285.

35. Wake, D. A. *et al.* The SDSS-IV MaNGA Sample: Design, Optimization, and Usage Considerations. *Astron. J.* **154**, 86 (2017). 1707.02989.

36. Smee, S. A. *et al.* The Multi-object, Fiber-fed Spectrographs for the Sloan Digital Sky Survey and the Baryon Oscillation Spectroscopic Survey. *Astron. J.* **146**, 32 (2013). 1208.2233.

37. Yan, R. *et al.* SDSS-IV/MaNGA: Spectrophotometric Calibration Technique. *Astron. J.* **151**, 8 (2016). 1511.01496.

38. Gunn, J. E. *et al.* The 2.5 m Telescope of the Sloan Digital Sky Survey. *Astron. J.* **131**, 2332–2359 (2006). astro-ph/0602326.

39. Abolfathi, B. *et al.* The Fourteenth Data Release of the Sloan Digital Sky Survey: First Spectroscopic Data from the Extended Baryon Oscillation Spectroscopic Survey and from the Second Phase of the Apache Point Observatory Galactic Evolution Experiment. *Astrophys. J. Suppl.* **235**, 42 (2018). 1707.09322.

40. Lintott, C. J. *et al.* Galaxy Zoo: morphologies derived from visual inspection of galaxies from the Sloan Digital Sky Survey. *Mon. Not. R. Astron. Soc.* **389**, 1179–1189 (2008). 0804.4483.

41. Lintott, C. *et al.* Galaxy Zoo 1: data release of morphological classifications for nearly 900 000 galaxies. *Mon. Not. R. Astron. Soc.* **410**, 166–178 (2011). 1007.3265.

42. Masters, K. & the MaNGA collaboration (2019, in preparation).

43. Vazdekis, A. *et al.* Evolutionary stellar population synthesis with MILES - II. Scaled-solar and α-enhanced models. *Mon. Not. R. Astron. Soc.* **449**, 1177–1214 (2015). 1504.08032.

44. Vazdekis, A. *et al.* Evolutionary stellar population synthesis with MILES - I. The base models and a new line index system. *Mon. Not. R. Astron. Soc.* **404**, 1639–1671 (2010). 1004.4439.

45. Kroupa, P. The Local Stellar Initial Mass Function. In Deiters, S., Fuchs, B., Just, A., Spurzem, R. & Wielen, R. (eds.) *Dynamics of Star Clusters and the Milky Way*, vol. 228 of *Astronomical Society of the Pacific Conference Series*, 187 (2001). astro-ph/0011328.

46. Girardi, L., Bressan, A., Bertelli, G. & Chiosi, C. Evolutionary tracks and isochrones for low- and intermediate-mass stars: From 0.15 to 7 M_{sun}, and from Z=0.0004 to 0.03. *Astron. & Astrophys. Suppl. Ser.* **141**, 371–383 (2000). astro-ph/9910164.

47. Cappellari, M. Improving the full spectrum fitting method: accurate convolution with Gauss-Hermite functions. *Mon. Not. R. Astron. Soc.* **466**, 798–811 (2017). 1607.08538.

48. Asari, N. V. *et al.* The history of star-forming galaxies in the Sloan Digital Sky Survey. *Mon. Not. R. Astron. Soc.* **381**, 263–279 (2007). 0707.3578.

49. Peterken, T. & the MaNGA collaboration (2019, in preparation).

50. Cardelli, J. A., Clayton, G. C. & Mathis, J. S. The relationship between infrared, optical, and ultraviolet extinction. *Astrophys. J.* **345**, 245–256 (1989).

51. Blanton, M. R., Kazin, E., Muna, D., Weaver, B. A. & Price-Whelan, A. Improved Background Subtraction for the Sloan Digital Sky Survey Images. *Astron. J.* **142**, 31 (2011). 1105.1960.

52. Gerssen, J., Kuijken, K. & Merrifield, M. R. The shape of the velocity ellipsoid in NGC 488. *Mon. Not. R. Astron. Soc.* **288**, 618–622 (1997). astro-ph/9702128.

53. Westfall, K. & the MaNGA collaboration (2018, in preparation).

A Acknowledgements

This work makes extensive use of the `Starlight` and `pPXF` spectral fitting tools, both of which are freely available. The `Starlight`[3] project is supported by the Brazilian agencies CNPq, CAPES and FAPESP and by the France-Brazil CAPES/Cofecub program. `pPXF`[4] was created and is maintained by Michele Cappellari. The table-matching tool `TOPCAT`[5] was also used in this work[27].

Several Python tools were also essential for this research. `Astropy`[6] is a community-developed core Python package for Astronomy.[28] `Scipy`[7] is an open-source scientific computing package.[29] The figures in this Letter were generated using `matplotlib`.[308]

This publication uses data generated via the Zooniverse.org platform, development of which is funded by generous support, including a Global Impact Award from Google, and by a grant from the Alfred P. Sloan Foundation. This publication has been made possible by the participation of almost 6000 volunteers in the Galaxy Zoo:3D project on Zooniverse.org.

Funding for the Sloan Digital Sky Survey IV has been provided by the Alfred P. Sloan Foundation, the U.S. Department of Energy Office of Science, and the Participating Institu-

[3]Available at `http://www.starlight.ufsc.br/`

[4]Available at `http://www-astro.physics.ox.ac.uk/~mxc/software/`

[5]Available at `http://www.star.bris.ac.uk/%7Embt/topcat/`

[6]Available at `http://www.astropy.org/`

[7]Available at `http://www.scipy.org/`

[8]Available at `https://matplotlib.org/`

tions. SDSS-IV acknowledges support and resources from the Center for High-Performance Computing at the University of Utah. The SDSS web site is `www.sdss.org`.

SDSS-IV is managed by the Astrophysical Research Consortium for the Participating Institutions of the SDSS Collaboration including the Brazilian Participation Group, the Carnegie Institution for Science, Carnegie Mellon University, the Chilean Participation Group, the French Participation Group, Harvard-Smithsonian Center for Astrophysics, Instituto de Astrofísica de Canarias, The Johns Hopkins University, Kavli Institute for the Physics and Mathematics of the Universe (IPMU) / University of Tokyo, Lawrence Berkeley National Laboratory, Leibniz Institut für Astrophysik Potsdam (AIP), Max-Planck-Institut für Astronomie (MPIA Heidelberg), Max-Planck-Institut für Astrophysik (MPA Garching), Max-Planck-Institut für Extraterrestrische Physik (MPE), National Astronomical Observatories of China, New Mexico State University, New York University, University of Notre Dame, Observatório Nacional / MCTI, The Ohio State University, Pennsylvania State University, Shanghai Astronomical Observatory, United Kingdom Participation Group, Universidad Nacional Autónoma de México, University of Arizona, University of Colorado Boulder, University of Oxford, University of Portsmouth, University of Utah, University of Virginia, University of Washington, University of Wisconsin, Vanderbilt University, and Yale University.

We are grateful for access to the University of Nottingham High Performance Computing Facility, without which the spectral fitting work done here would not have been possible

in any reasonable timeframe.

B Author contributions

M.M. conceived of the presented idea. T.P. developed the method and obtained the results. A.A.S. and M.M. supervised the work and led the main analysis and interpretation with T.P.. K.W. calculated the kinematic parameters of UGC 3825 and discussed the implications of the results presented here. K.M. and C.K. devised, implemented, and provided output from the Galaxy Zoo:3D spiral arm mask project. N.D., K.M., A.W., K.W., and many others in the SDSS community obtained the MaNGA IFU data, developed reduction and analysis code, continue to maintain software and hardware, and performed many other tasks necessary for the running of a large collaboration. All authors discussed the results and contributed to the final manuscript.

C Methods

MaNGA The SDSS-IV MaNGA survey[31,32] provides integral-field spectroscopy[33,34] for a large sample of low-redshift galaxies[35] using the BOSS spectrograph[36,37] on the SDSS telescope[38] located at Apache Point, New Mexico. Please refer to referenced publications on the technical specifications of the survey[31–38].

This work makes use of the IFS mapping of UGC 3825 (MaNGA plate-IFU 8132-12702), which is publicly available as part of the fourteenth SDSS data release (DR14)[39]. As part of

this work, we make use of the MaNGA data analysis pipeline (DAP) outputs as part of the internal data release MPL-6. These DAP outputs will be publicly available as part of SDSS DR15, planned for December 2018.

Galaxy Zoo:3D Figure 1 makes use of spiral arm masks generated by Galaxy Zoo:3D (GZ:3D) as a fiducial. This is an ongoing citizen science project inspired by the Galaxy Zoo[40,41] galaxy classification project. In GZ:3D, volunteer users are shown images of galaxies in the MaNGA target catalogue and are asked to draw boundaries marking the edges of spiral arms and bars, as well as identifying the position of the galactic centre. The end result is an image with defined spiral and bar weights at each position, determined by the number of users who defined that position as part of a spiral arm or a bar. Further details will be published in a separate paper[42]. For UGC 3825, 8 users drew spiral arms, so the fiducial in Figure 1 is a contour denoting the contiguous region where at least 2 users defined as being part of the spiral arms.

Spectral fitting MaNGA data provide a cube of information comprising a spectrum at each spatial location on the sky. Each such spectrum of UGC 3825 (MaNGA plate-IFU 8132-12702) was fitted using a set of 270 single stellar population (SSP) template spectra from the MILES project[43,44]. These templates were chosen to cover a wide range of ages (27 values between $10^{7.5}$ years and $10^{10.1}$ years) and metallicities (10 values of [M/H] between -1.79 and +0.40). The finer sampling of the age parameter space was required to achieve the temporal resolution needed to separate out the young stellar components sought in this

analysis; the coarser sampling in metallicity is entirely adequate for this work while keeping the total number of templates within the maximum that the software can process. We assume a Kroupa revised stellar initial mass function (IMF)[45] with Padova isochrones[46]. We fit each spaxel spectra individually to ensure that we retain all of the spatial information possible. This will result in decreased signal-to-noise (S/N) at the edges of the galaxy, but within the region indicated in Figure 2, no spaxel has a S/N less than 4.2. Noise at a pixel-by-pixel basis is smoothed out by the cross-correlation techniques in any case. No regularization was imposed on any of the fitting processes.

As a first step to extract and remove emission-line contributions from the spectra, `pPXF`[20,47] was used to simultaneously fit the shape and kinematics of both the stellar spectra and a full set of emission lines, whose profiles were assumed to be Gaussian. The resulting Hα emission-line flux measurements provide the tracer of ongoing star formation, since Hα luminosity $L_{\mathrm{H}\alpha}$ is directly proportional to the local star-formation rate[19].

The spectra were initially logarithmically binned to allow the kinematics to be derived. After the emission lines had been subtracted out, the remaining stellar spectra were rebinned to a linear scale and fitted using the `Starlight`[18,48] code that is optimised for modelling stellar populations.[9] To reproduce the observed spectra in the fitting process, we also allowed for dust obscuration using a variable-strength Calzetti, Clayton & Mathis reddening law.[50].

[9] Although `Starlight` is explicitly designed for this task, a cross check of the results from the `Starlight` and `pPXF` codes confirmed very close agreement between the stellar population results obtained.[49]

The resulting output from `Starlight` provides the contribution of each SSP of specific age and metallicity to the spectrum at each location across the face of the galaxy. Thus, we can extract a map of the contribution of stars with differing properties to the total light from the galaxy. In this case, we are interested in mapping out the young stars, so we extract the contribution to the total light from all the SSPs with ages of less than 6×10^7 years. These will be mainly O- and B-type stars, with an average luminosity-weighted age of $\approx 2 \times 10^7$ years.

Measuring the offset Although the angular offset $\delta\theta(r)$ between the maps of young stars and Hα emission is visually apparent in the data (See Figure 1), it is quite a subtle effect, so some care must be taken to optimise the signal when extracting it. As a first step, we deproject the maps to face-on using kinematic centre, inclination, and position angle measurements, determined from the best-fit parameters to the gas disk kinematics, and convert the Cartesian images to polar ones, binned in radius with a step-size of $\Delta r \approx$ 0.16 kpc. When the NASA-Sloan Atlas[51] measurements are used instead for the centre, inclination and position angles (assuming the galaxy disk is intrinsically round), the results are unchanged.

For each such radius, we determine the offset between the spiral features in the Hα and young-stellar map by cross-correlating the signal in the polar maps, displayed in Figure 3. The location of the cross-correlation maximum was then refined to a sub-pixel value by fitting a 2^{nd}-order polynomial around the peak. The region of $r < 3.2$ kpc (approximately

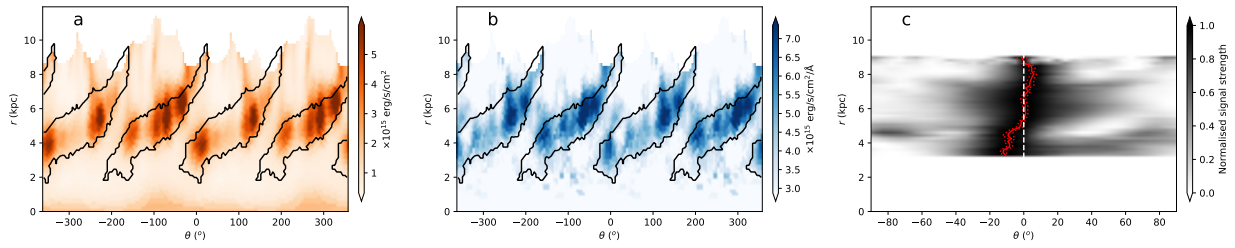

Figure 3: Polar-coordinate maps of the Hα emission line (*left*) and young stars (*centre*). The galactic centre is at the bottom of the map, and the black outlines indicate the location of the same GZ:3D spiral arm mask used in Figure 1. The cross-correlation signal between these maps is also shown (*right*), with the cross-correlation angle $\delta\theta(r)$ shown as a red line.

$0.32R_E$) in Figures 2 and 3 is ignored when calculating $\Omega_{\rm P}(r)$ since the azimuthal signal of Hα variations here is found to be too small to reliably measure $\delta\theta(r)$.

A conservative estimate for the uncertainty $\delta_{\Delta\theta}(r)$ in this offset can be obtained from the ratio of the full-width-at-half-maximum (FWHM) of the peak in the cross-correlation signal to the signal-to-noise ratio (SNR) of the signal. The SNR is in turn estimated as the ratio of the peak height H to the standard deviation of the cross-correlation signal $\sigma_{\delta\theta(r)}$; i.e.

$$\delta_{\Delta\theta}(r) = \frac{\mathrm{FWHM}(r) \times \sigma_{\delta\theta(r)}}{H(r)}. \tag{2}$$

The radially-varying FWHM allows the value of $\delta_{\Delta\theta}(r)$ to account for the radial variation in the MaNGA beam size effects in the polar-coordinate plots. At low r, the beam covers a large range in θ. The cross-correlation signal's peak will therefore be proportionally wider, increasing $\delta_{\Delta\theta}(r)$. At large radius, the beam will cover a small range in θ, allowing us to

obtain a tighter constraint on the value of $\delta\theta(r)$.

Measuring the angular velocity of circular orbits The other ingredient needed to determine the pattern speed is the angular speed of material following a circular orbit in the galaxy. We use gas velocity measurements to determine the angular velocity of material $\Omega(r)$ since the very young stars this material traces will not yet have been dynamically heated from their purely circular trajectories[52]. The MaNGA data analysis pipeline (DAP)[53] provides measurements of the line-of-sight gas velocity $v_{\rm los,gas}$ for each pixel. This analysis uses the MPL-6 version of the DAP outputs.

Using the same process as described above, the $v_{\rm gas}$ map can be remapped into polar coordinates. At each radius, the observed line-of-sight velocity will vary sinusoidally with azimuthal angle, and a simple least-squares fit yields the amplitude of this variation at each radius, $V_{\rm gas}(r)$. The angular speed can then be simply calculated as $\Omega(r) = \frac{V_{\rm gas}(r)}{r \times \sin(i)}$, where i is the inclination angle of the galaxy to the line of sight ($i = 0$ for a face-on galaxy) derived from the observed ellipticity in the NASA-Sloan Atlas. The error in Ω is dominated by the contribution from the uncertainty in the sinusoidal fit, and so this value is adopted.

Testing with an older stellar population If the picture established here is correct, then it should be possible to repeat the analysis using a somewhat older stellar population that will have had time to travel further from the peak of the spiral density wave. In practice, it appears that the residual spiral feature fades very rapidly into the noise from the more general disk population, but we were able to extract a consistent signal from a portion of the

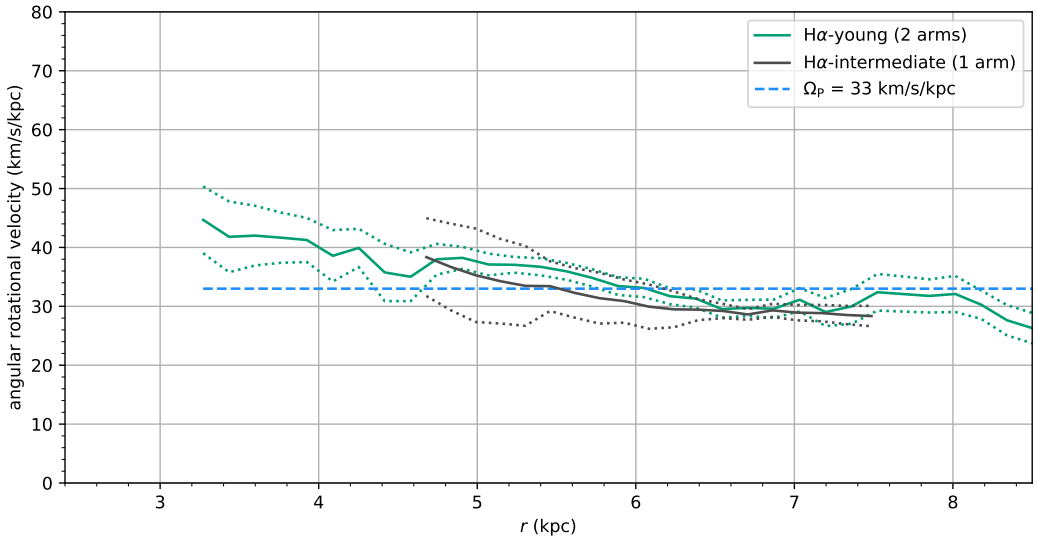

Figure 4: As Figure 2; $\Omega_{\rm P}(r)$ derived in the main text (blue solid) with a best-fit flat line (light blue dashed), and also showing $\Omega_{\rm P}(r)$ derived from the offset between Hα and the stars of age 0.2 to 1.3 Gyr in the southern arm (pink).

southern spiral arm for an intermediate-age population combining the templates with ages between 0.2 and 1.3 Gyr. This population mainly comprises B- and A-type stars; adopting a luminosity-weighted age of $\approx 2 \times 10^8$ years, the results from the angular offset of these somewhat older stars, shown in Figure 4, are entirely consistent with the pattern speed derived in the main text, giving some further confidence in both the method and the density wave theory.